



## Effective cloud fractions from the Ozone Monitoring Instrument: Theoretical framework and validation

P. Stammes,<sup>1</sup> M. Sneep,<sup>1</sup> J. F. de Haan,<sup>1</sup> J. P. Veefkind,<sup>1</sup> P. Wang,<sup>1</sup> and P. F. Levelt<sup>1</sup>

Received 15 April 2007; revised 8 January 2008; accepted 25 February 2008; published 5 June 2008.

[1] The Dutch-Finnish Ozone Monitoring Instrument (OMI) on board NASA's EOS-Aura satellite is measuring ozone, NO<sub>2</sub>, and other trace gases with daily global coverage. To correct these trace gas retrievals for the presence of clouds, there are two OMI cloud products, based on different physical processes, namely, absorption by O<sub>2</sub>-O<sub>2</sub> at 477 nm (OMCLDO2) and rotational Raman scattering (RRS) in the UV (OMCLDRR). Both cloud products use a Lambertian cloud model with albedo 0.8 and contain the effective (i.e., radiometric) cloud fraction and the cloud pressure. First, the theoretical framework for the Lambertian cloud model is given and the concept of effective cloud fraction is discussed. Next, an intercomparison of the effective cloud fractions from both products is presented, as well as a comparison with MODIS cloud data. It is shown that the O<sub>2</sub>-O<sub>2</sub> and RRS effective cloud fractions correlate very well (95%) but that there is an offset of about 0.10. From MODIS geometric cloud fraction and cloud optical thickness data a MODIS effective cloud fraction was calculated. The effective cloud fractions from OMCLDO2 and MODIS show a high correlation of 92% with a very small offset (0.01). In order to guide users, a summary of the validation status of effective cloud fraction and cloud pressure from the OMCLDO2 and OMCLDRR cloud products is presented.

**Citation:** Stammes, P., M. Sneep, J. F. de Haan, J. P. Veefkind, P. Wang, and P. F. Levelt (2008), Effective cloud fractions from the Ozone Monitoring Instrument: Theoretical framework and validation, *J. Geophys. Res.*, 113, D16S38, doi:10.1029/2007JD008820.

### 1. Introduction

[2] Global ozone monitoring from satellite started almost 30 years ago with the Total Ozone Mapping Spectrometer (TOMS) on Nimbus 7. The series of TOMS instruments on three different satellites (Nimbus 7, 1978–1993; Meteor-3, 1992–1994; and Earth Probe, 1996–2005) provide a prime satellite data record for chemistry and climate. The Dutch-Finnish Ozone Monitoring Instrument (OMI), launched on 15 July 2004 on board of NASA's EOS-Aura mission, continues the TOMS data record for total ozone and other atmospheric parameters related to ozone chemistry and climate.

[3] OMI is a UV-visible spectrometer covering the wavelength range 270–500 nm, with a spectral resolution of 0.42–0.63 nm. With these spectral capabilities OMI is suited to detect several other gases besides ozone, like NO<sub>2</sub>, SO<sub>2</sub>, and HCHO, and aerosols. The swath is wide enough to allow for global coverage in 1 d, with a spatial resolution of 13 × 24 km<sup>2</sup> for nadir observations. With these capabilities OMI contributes to global air quality monitoring. The heritage for the design of OMI and its trace gas retrieval techniques comes, apart from TOMS, from Global Ozone Monitoring Experiment (GOME) launched in 1995 [Burrows *et al.*, 1999], and Scanning

Imaging Absorption Spectrometer for Atmospheric Cartography (SCIAMACHY) launched in 2002 [Bovensmann *et al.*, 1999]. A detailed description of the OMI instrument and its science objectives is given by Levelt *et al.* [2006a, 2006b].

[4] Clouds form one of the most important factors that can potentially limit the accuracy of OMI's trace gas measurements, both for stratospheric and tropospheric gases. Since clouds are ubiquitous, they must be detected and possibly be corrected for in the trace gas retrievals. Because the OMI radiance spectrum contains information about tropospheric gases also in case of partial cloudiness or thin clouds, we need to exploit this information as well as possible. The effects of clouds on trace gas retrievals are basically threefold: (1) in the albedo effect, clouds enhance the importance of single and multiple scattering light paths from Sun to cloud to satellite, as compared to Rayleigh scattering light paths; for low clouds this leads to enhanced absorption in the gas layer above the cloud, and thereby to increased depth of absorption lines as compared to the clear sky; (2) in the shielding effect, clouds shield the tropospheric gases below them; this is often compensated for by the addition of a so-called ghost column; and (3) in the in-cloud absorption effect, scattering by cloud particles increases the light path inside the cloud, and thus the depth of absorption lines of gases present in the cloud as compared to a nonscattering layer. The effects of clouds on ozone retrievals have been studied using radiative transfer modeling by, among others, Newchurch *et al.* [2001], Liu *et al.* [2004], and Ahmad *et al.* [2004] for TOMS and by

<sup>1</sup>Climate Research and Seismology Department, Royal Netherlands Meteorological Institute, De Bilt, Netherlands.

*Koelemeijer and Stammes* [1999] and *Kokhanovsky et al.* [2007] for GOME and SCIAMACHY; the effects of clouds on NO<sub>2</sub> retrievals have been studied by *Boersma et al.* [2004] and *Wang et al.* [2006]. From these studies it followed that the cloud fraction, cloud albedo, and cloud pressure are important quantities for cloud correction. Errors in these cloud products will directly end up in errors in ozone [*Vasilkov et al.*, 2004; *Joiner et al.*, 2006] and NO<sub>2</sub> [*Boersma et al.*, 2004].

[5] In order to detect clouds from OMI spectra and to correct for their presence in trace gas retrievals, there are two OMI cloud products. These are based on the same physical principle, namely, determination of the mean photon path in the UV-visible from analysis of a spectral feature of a well-mixed species. However, the products use different physical processes: the O<sub>2</sub>–O<sub>2</sub> cloud product OMCLDO2 [*Acarreta et al.*, 2004; *Sneep et al.*, 2008] uses the 477 nm absorption line of O<sub>2</sub>–O<sub>2</sub> (collision induced absorption by oxygen), whereas the rotational Raman scattering (RRS) cloud product OMCLDRR [*Joiner et al.*, 2004; *Joiner and Vasilkov*, 2006; *Vasilkov et al.*, 2008] uses the filling-in of Fraunhofer lines in the UV due to rotational Raman scattering by air molecules; the current OMCLDRR window is 345–354 nm. Both cloud algorithms use a simplified Lambertian cloud model, and produce two parameters: effective cloud fraction, using an assumed cloud albedo of 0.8, and cloud pressure.

[6] The purpose of this paper is to show an intercomparison of the effective cloud fractions from the OMI O<sub>2</sub>–O<sub>2</sub> and RRS products for 1 day of global data. In addition, a global comparison is shown with the MODIS/Aqua cloud fraction. The intercomparison of the cloud pressures from the two OMI cloud products is presented by *Sneep et al.* [2008], as well as comparison with PARASOL, MODIS/Aqua, and CloudSat cloud pressures. Comparisons between OMI RRS cloud pressures and MODIS and CloudSat data are also shown by *Vasilkov et al.* [2008]. The validation approach is to use collocated data from cloud sensors on board other satellites in the A train. This is a powerful use of the synergy of the A-train instruments and leads to a significant validation result with data acquired over only a short period of time.

[7] The structure of the paper is as follows. In section 2 we explain the Lambertian cloud model, discuss the effective cloud fraction concept, and show the impact of the Lambertian cloud model on total ozone retrieval from simulations. In section 3 the OMI cloud algorithms are briefly described. In section 4 the effective cloud fractions from the two cloud algorithms are compared using 1 day of global data. In section 5 the comparison between OMI O<sub>2</sub>–O<sub>2</sub> and MODIS cloud fraction is given. In section 6 the discussion and conclusions are presented, including an overview of the OMI cloud product comparisons with other A-train cloud data presented in the special Aura Validation section.

## 2. Rationale for the Lambertian Cloud Model in Trace Gas Retrievals

[8] Satellite spectrometers for trace gas detection operating in the UV-visible, like OMI, GOME, SCIAMACHY, and GOME-2, have a relatively coarse spatial resolution, ranging from 13 × 24 km<sup>2</sup> to 40 × 320 km<sup>2</sup>. These

instruments do not resolve individual clouds as satellite imagers with a 1 × 1 km<sup>2</sup> resolution, like MODIS, do. Therefore, only a small percentage of the observed pixels (5–15%) are cloud free [*Krijger et al.*, 2007]; most pixels are either fully or partly cloudy. Therefore we assume that a pixel consists of a cloudy part, with geometric fraction  $c$ , and a clear part with geometric fraction  $1 - c$ . We use the independent pixel approximation, in which the pixel reflectance is the sum of the reflectances of the cloudy part, weighted by  $c$ , and the clear part, weighted by  $1 - c$ .

[9] The four most important cloud parameters for trace gas correction are the parameters that determine the photon paths in the atmosphere. These parameters are the geometric cloud fraction  $c$ , the cloud optical thickness  $\tau_c$ , the cloud top altitude  $z_{c,top}$ , and the cloud vertical extent  $h$ , which is equal to  $z_{c,top} - z_{c,bot}$ . Because of the limited spatial resolution, the geometric cloud fraction and the cloud optical thickness cannot be separated: an optically thick cloud with a small geometric cloud fraction can yield the same top-of-atmosphere (TOA) reflectance as an optically thin cloud with a large geometric cloud fraction. So we have to fix either the geometric cloud fraction or the cloud optical thickness. Furthermore, there are several cloud parameters on which we have no information from OMI, e.g., cloud phase, cloud particle shape and size, and cloud vertical structure, so we prefer to use a simple cloud model. Because clouds are a correction step in trace gas retrievals, both the cloud retrieval algorithm and the cloud correction algorithm should use the same cloud model. A simple cloud model improves the speed of both algorithms. We therefore assume a Lambertian reflector with a fixed albedo through which no light is transmitted as the simplified cloud model. The fraction of this Lambertian cloud covering the pixel is called the effective cloud fraction,  $c_{eff}$ . The effective cloud fraction is not the geometric cloud fraction of the true cloud but the radiometrically equivalent cloud fraction, which in combination with the assumed cloud albedo yields a TOA reflectance that agrees with the observed reflectance.

[10] Because of limited spectral information in the O<sub>2</sub>–O<sub>2</sub> absorption band and the RRS process that are used for cloud pressure retrieval, the cloud top altitude and the cloud vertical extent cannot be separated. Therefore, we use only one altitude parameter, namely, the altitude level of the Lambertian cloud,  $z_c$ . The level of the Lambertian cloud is adjusted so that the retrieved cloud yields the same amount of signal (either amount of O<sub>2</sub>–O<sub>2</sub> absorption, or amount of Raman scattering) as the observation. A sketch of a scattering cloud pixel and a Lambertian cloud pixel is shown in Figure 1.

[11] Both OMI cloud retrieval algorithms use the Lambertian cloud model with an assumed albedo of 0.8. The same cloud model is used in the TOMS ozone algorithm [*McPeters et al.*, 1996] and in the O<sub>2</sub> A-band cloud retrieval method FRESCO [*Koelemeijer et al.*, 2001], which has been applied to GOME, SCIAMACHY and GOME-2. Comparisons with simulations of scattering clouds have shown that the high cloud albedo of 0.8 is a suitable value in order to correct total ozone and NO<sub>2</sub> retrievals for clouds [*Koelemeijer and Stammes*, 1999; *Ahmad et al.*, 2004; *Vasilkov et al.*, 2004; *Wang et al.*, 2006]. The high albedo of the Lambertian cloud model is chosen such that most scenes have an effective cloud fraction less than 1 (because most clouds have an albedo less than 0.8), and such that the

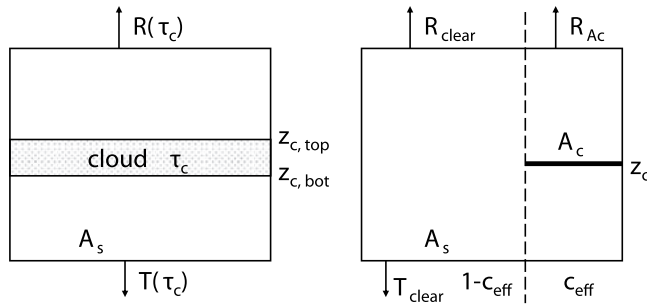


**Figure 1.** Sketch (side view) of (left) a pixel with a scattering cloud model and (right) a pixel with a Lambertian cloud model which is used in the OMI cloud retrieval and cloud correction algorithms.

missing transmission of optically thin and medium thick clouds in the Lambertian cloud model is compensated for by the large cloud-free part of the pixel.

## 2.1. Choice of Lambertian Cloud Albedo

[12] A quantitative rationale for the choice of 0.8 for the albedo of the Lambertian cloud model is as follows. Scattering clouds have two main optical properties in the UV-visible, namely, reflection and transmission; their absorption is negligible. A Lambertian reflector has only reflection properties, determined by the cloud albedo, and no transmission properties. Therefore, the missing transmission of the Lambertian cloud must be compensated for by the cloud-free part of the pixel,  $1 - c_{\text{eff}}$ . Let us assume a fully cloudy pixel ( $c = 1$ ) with cloud optical thickness  $\tau_c$ . We wish to approximate the reflection  $R(\tau_c)$  and transmission  $T(\tau_c)$  of this scattering cloud pixel by the reflection  $R_L$  and transmission  $T_L$  of a Lambertian cloud pixel, with cloud albedo  $A_c$  and cloud fraction  $c_{\text{eff}}$ . If we can approximate both the reflection and transmission properties of the scattering cloud by a partially covered Lambertian cloud pixel, we have an optimal Lambertian cloud model. Since reflection and transmission of a scattering cloud are directionally dependent, we consider for simplicity the reflection and transmission properties averaged over solar and viewing directions, i.e., the spherical albedo  $R^s$  and spherical transmission  $T^s$ . We now have two equations with two unknowns,  $A_c$  and  $c_{\text{eff}}$ :

$$R^s(\tau_c) = R_L^s = (1 - c_{\text{eff}})R_{\text{clear}}^s + c_{\text{eff}}R_{A_c}^s \quad (1)$$

$$T^s(\tau_c) = T_L^s = (1 - c_{\text{eff}})T_{\text{clear}}^s, \quad (2)$$

where  $R_{\text{clear}}^s$  and  $T_{\text{clear}}^s$  are the clear sky spherical albedo and transmission, respectively, which depend on the Rayleigh and aerosol optical thickness and the surface albedo,  $A_s$ .  $R_{A_c}^s$  is the TOA spherical albedo for a scene with a Lambertian cloud with albedo  $A_c$ . In equation (2) we have used the fact that the cloudy part of  $T_L^s$  has zero transmission. Combining equations (1) and (2), we get for the spherical albedo of the Lambertian cloud part of the pixel:

$$R_{A_c}^s = \frac{R^s(\tau_c)T_{\text{clear}}^s - T^s(\tau_c)R_{\text{clear}}^s}{T_{\text{clear}}^s - T^s(\tau_c)}. \quad (3)$$

Since  $c_{\text{eff}}$  is the free parameter in the cloud retrievals, determined from the observed reflectance, we only consider here  $A_c$ , which is the fixed parameter in the retrievals. This parameter can be selected using equation (3). Therefore, we performed calculations of  $R^s(\tau_c)$  and  $T^s(\tau_c)$  using the DAK (Doubling-Adding KNMI) multiple scattering model [*de Haan et al., 1987; Stammes, 2001*], for a single cloud layer with optical thickness  $\tau_c$  ranging from 1 to 100 and a Henyey-Greenstein phase function with asymmetry parameter 0.85, embedded between 1 and 2 km altitude in a Rayleigh scattering atmosphere. Some background aerosol (with optical thickness  $\tau_{\text{aer}} = 0.2$  at 330 nm and 0.1 at 470 nm) was added in the lowest kilometer of the atmosphere. Next we derived  $R_{A_c}^s$  using equation (3). In Figure 2,  $R_{A_c}^s$  is shown as a function of cloud optical thickness at three wavelengths relevant for OMI: 470 nm ( $\text{O}_2\text{-O}_2$  and  $\text{NO}_2$  retrieval windows), 350 nm (RRS retrieval window), and 330 nm (total ozone retrieval window). The surface albedo,  $A_s$ , is assumed to be 0.05 at all wavelengths; however, there is very little dependency of  $R_{A_c}^s$  on  $A_s$ . One observes that  $R_{A_c}^s$  is only weakly depending on  $\tau_c$  and lies in the range of 0.7–1.0; for a typical cloud optical thickness of 5,  $R_{A_c}^s$  is 0.8 at 330 nm and 0.9 at 350 and 470 nm. The difference is mainly due to the absorption by ozone at 330 nm. We note that for these high values of  $R_{A_c}^s$ ,  $A_c$  is almost equal to  $R_{A_c}^s$  at 470 nm and 350 nm; the difference is  $\leq 0.01$ . However, at 330 nm, where absorption by ozone takes place,  $A_c$  is higher than  $R_{A_c}^s$  by about 0.06 at  $R_{A_c}^s = 0.8$ . We conclude that with the choice of  $A_c = 0.8\text{--}0.9$  for the Lambertian cloud albedo, the missing transmission of the Lambertian cloud is compensated quite well by the increased transmission of the cloud-free part of the pixel. To remain consistent with currently used Lambertian cloud models, the Lambertian cloud albedo 0.8 is selected for OMI. If the pixel is not fully cloud covered ( $c < 1$ ), the same rationale for the choice of  $A_c$  holds, but then the retrieved value of  $c_{\text{eff}}$  should be multiplied by  $c$ .

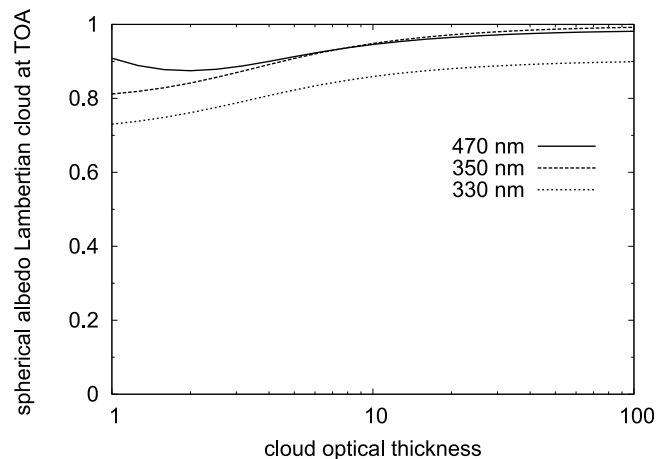


**Figure 2.** Spherical albedo at TOA of a Lambertian cloud,  $R_{A_c}^s$ , as a function of the optical thickness of a scattering cloud. Here the Lambertian cloud albedo  $A_c$  is calculated such that both the spherical reflection and transmission of the scattering cloud with a geometric cloud fraction of 1 are reproduced by a pixel with a Lambertian cloud with cloud fraction  $c_{\text{eff}}$ . The results are given for three relevant OMI wavelengths: 470, 350, and 330 nm.

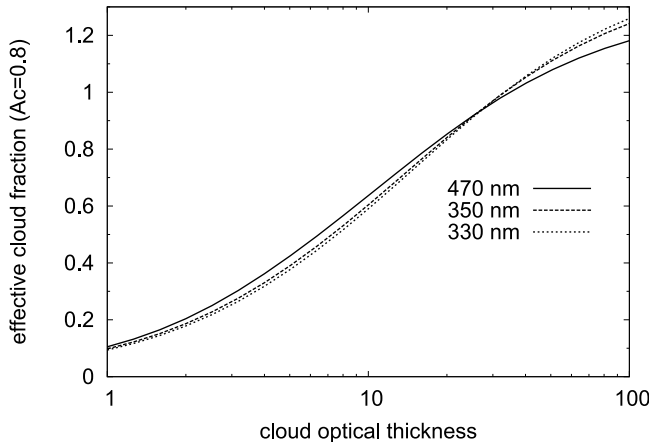


**Figure 3.** Effective cloud fraction  $c_{\text{eff}}$ , assuming a Lambertian cloud with albedo  $A_c = 0.8$ , as a function of the optical thickness of a scattering cloud having a geometric cloud fraction of 1. The results are given for the three relevant OMI wavelengths. Here  $c_{\text{eff}}$  is averaged over all viewing directions at solar zenith angle  $45^\circ$ ; the surface albedo is  $A_s = 0.05$ .

[13] This choice of Lambertian cloud model should lead to a good cloud correction of trace gas retrievals, which is discussed in section 2.3.

## 2.2. Effective Cloud Fraction Formulation

[14] In the OMI cloud retrieval algorithms the effective cloud fraction  $c_{\text{eff}}$  is determined from a fit of the Lambertian cloud model reflectance to the observed reflectance at the continuum wavelengths in the  $\text{O}_2\text{-O}_2$  and RRS retrieval windows around 470 and 350 nm, respectively. The “operational” definition of the effective cloud fraction is the amount of Lambertian cloud with albedo  $A_c$  that one has to add to the clear pixel to explain the observed reflectance under the given solar and viewing geometry, at the wavelength under consideration. A formal definition of  $c_{\text{eff}}$  can be formulated as follows. The observed TOA reflectance of a partly cloudy pixel can be written as the weighted sum of the reflectances of the cloudy and the clear parts:

$$R_{\text{obs}} = cR(\tau_c) + (1 - c)R_{\text{clear}}, \quad (4)$$

where  $R(\tau_c)$  is the cloudy reflectance and  $R_{\text{clear}}$  is the clear sky reflectance. The simulated TOA reflectance, using the Lambertian cloud model, can be written analogously as

$$R_{\text{sim}} = R_L = c_{\text{eff}}R_{A_c} + (1 - c_{\text{eff}})R_{\text{clear}}. \quad (5)$$

By imposing  $R_{\text{sim}} = R_{\text{obs}}$  we obtain the effective cloud fraction formula

$$c_{\text{eff}} = c \frac{R(\tau_c) - R_{\text{clear}}}{R_{A_c} - R_{\text{clear}}}. \quad (6)$$

As discussed in section 2.1, we use  $A_c = 0.8$ , so  $R_{A_c} \approx 0.8$ . The effective cloud fraction is proportional to the geometric cloud fraction  $c$ , with the proportionality factor depending most strongly on the cloud optical thickness  $\tau_c$  but also on the clear sky reflectance properties. The proportionality factor is the difference between the scattering cloud

reflectance and the clear sky reflectance,  $R(\tau_c) - R_{\text{clear}}$ , normalized by the difference between the Lambertian cloud reflectance and the clear sky reflectance,  $R_{A_c} - R_{\text{clear}}$ . This proportionality factor is shown in Figure 3, where the effective cloud fraction is shown for  $c = 1$  as a function of  $\tau_c$ , for the three relevant OMI wavelengths, 470, 350, and 330 nm. Here the surface albedo is assumed to be 0.05.

[15] It is important to note that whereas  $c$  is independent of wavelength,  $c_{\text{eff}}$  is wavelength-dependent, because the reflectances on the right-hand side of equation (6) are spectral quantities. Although  $R(\tau_c)$  is almost constant throughout the UV-visible,  $R_{\text{clear}}$  is not, since it is determined by Rayleigh scattering, which is strongly wavelength-dependent. This spectral dependence of  $c_{\text{eff}}$  can be seen in Figure 3 for 470, 350, and 330 nm. The effective cloud fraction increases with wavelength for  $\tau_c < 30$  (around which value  $R(\tau_c) = 0.8$ ) and decreases with wavelength for larger  $\tau_c$ . This behavior can be understood from equation (6), since for larger wavelengths  $R_{\text{clear}}$  is decreasing due to the decrease in Rayleigh scattering. As a result, the dependence of  $c_{\text{eff}}$  on  $\tau_c$  for the three wavelengths shows small offsets. The difference in  $c_{\text{eff}}$  between 470 and 350 nm is  $< 0.04$  for  $\tau_c < 30$ . The difference in  $c_{\text{eff}}$  between 350 and 330 nm is  $< 0.02$ . The behavior of  $c_{\text{eff}}$  for 750 nm (not shown), which is relevant for the  $\text{O}_2$  A band as observed by GOME and SCIAMACHY, is very close ( $< 0.02$ ) to the behavior for 470 nm at the full range of  $\tau_c$ .

[16] Because of the spectral dependence of  $c_{\text{eff}}$  one cannot directly use the value from the cloud retrieval window in the ozone retrieval window. Therefore, in the OMI DOAS ozone retrieval algorithm [Veeffkind *et al.*, 2006],  $c_{\text{eff}}$  at 330 nm is varied such that the simulated TOA reflectance fits the observed reflectance in the ozone window.

[17] We performed similar calculations for a surface albedo of 0.2 and found that in that case the behavior of  $c_{\text{eff}}$  versus  $\tau_c$  at 470 nm is very similar to that for surface albedo of 0.05 but with  $c_{\text{eff}}$  shifted to smaller values by at most 0.025 for  $\tau_c < 30$ .

[18] The effective cloud fraction and Lambertian cloud albedo are used in the cloud correction step of DOAS trace gas retrievals from OMI. In DOAS retrievals the so-called air mass factor [Burrows *et al.*, 1999; Palmer *et al.*, 2001] plays a key role. The air mass factor is the mean photon path in the atmosphere at the absorption line wavelength, and depends largely on the geometry, the atmospheric scattering properties and trace gas vertical profile. The air mass factor of a partly cloudy pixel is the weighted sum of the air mass factors of the clear and cloudy parts of the pixel [Palmer *et al.*, 2001; Boersma *et al.*, 2004; Van Roozendaal *et al.*, 2006; Veeffkind *et al.*, 2006]. The weight of the air mass factor of the cloudy part is the fractional reflectance due to clouds in the pixel, and thus given by (see equations (4) and (5))

$$w = \frac{c_{\text{eff}}R_{A_c}}{R_{\text{obs}}}. \quad (7)$$

So the retrieval of the effective cloud fraction under the assumption of a Lambertian cloud with albedo  $A_c$  is equivalent to the retrieval of the air mass factor weight  $w$  of the cloudy part of the pixel.

[19] The same Lambertian cloud model with  $A_c = 0.8$  is used in most OMI trace gas retrieval algorithms. This means

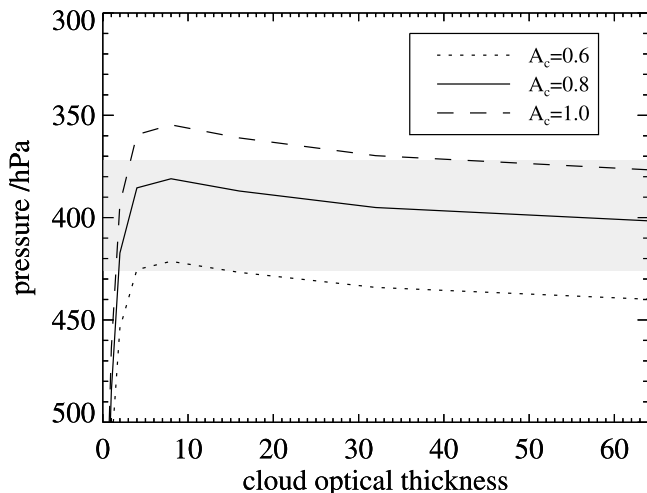


**Figure 4.** Retrieved cloud pressure from the  $O_2-O_2$  cloud algorithm as a function of the optical thickness of the scattering cloud for three values of the albedo of the Lambertian cloud. The surface albedo is 0.05, the geometrical cloud fraction of the scattering cloud is 0.5, and the cloud is located between 7 and 8 km (at 426 and 372 hPa, respectively). The viewing zenith angle is  $30^\circ$ , the solar zenith angle is  $60^\circ$ , and the azimuth difference is  $90^\circ$ .

that bidirectional effects of real clouds on  $c_{\text{eff}}$ , and possibly other errors that are due to the simplified cloud model, are compensated for to first order if the cloud product is used in a consistent way.

### 2.3. Effect of Lambertian Clouds on Ozone Column Retrieval

[20] We show here the effect of the Lambertian cloud model instead of a scattering cloud model for ozone column retrieval from radiative transfer simulations. We use a scattering cloud model for the simulation of the reflectance of a cloudy pixel in both the  $O_2-O_2$  cloud retrieval window and the ozone retrieval window. We next apply the Lambertian cloud retrieval model to these simulations and show the influence of the cloud model on the accuracy of the ozone column retrieval. The calculations were performed for a Henyey-Greenstein scattering cloud with asymmetry parameter  $g = 0.85$ , embedded in a Rayleigh scattering atmosphere between 7 and 8 km. A midlatitude summer ozone profile was used, the surface albedo was 0.05 and the geometric cloud fraction for the scattering cloud was 0.5. Calculations were performed at 477 nm for  $O_2-O_2$  absorption and at 333 nm for ozone absorption. The effective cloud fraction and cloud pressure were obtained by demanding that the reflectance in both spectral windows was reproduced when a Lambertian cloud model replaced the scattering cloud. Next the air mass factor for ozone was calculated using the Lambertian cloud model. Comparison of this air mass factor with the one for the scattering cloud model provides us with the relative error in the total ozone column due to the use of a Lambertian cloud located at a cloud pressure that is derived from the  $O_2-O_2$  cloud algorithm.

[21] Figures 4 and 5 show the retrieved cloud pressure and the relative error in the total ozone column as a function of the cloud optical thickness, respectively. Results are

given for three different values of  $A_c$ : 0.6, 0.8, and 1.0. Figure 4 shows that the retrieved cloud pressure depends strongly on the assumed value of  $A_c$ . If the cloud albedo is 0.6, we often retrieve a level close to the bottom of the cloud; if it is 1.0, we often retrieve a level near the top of the cloud. For cloud albedo 0.8 we find a level inside the cloud; only if the cloud is very tenuous, with cloud optical thickness  $\tau_c < 2$ , the retrieved cloud pressure is below the cloud. For larger cloud optical thicknesses the retrieved pressure is close to the optical midlevel of the cloud, with a broad minimum in retrieved cloud pressure around  $\tau_c = 10$ . This behavior of the retrieved cloud pressure as a function of cloud optical thickness for larger  $\tau_c$  is due to multiple scattering effects: if the cloud optical thickness increases, the mean photon path increases proportionally [van de Hulst, 1980, section 17.2.3].

[22] As mentioned above, previous studies showed that a Lambertian cloud albedo of 0.8 is a suitable value in order to have small ozone retrieval errors. Figure 5 confirms this value for clouds that have an optical thickness up to about 30. For larger optical thicknesses it might be better to choose a cloud albedo of 0.9. This is in agreement with the findings from section 2.1.

[23] We repeated the calculations for different geometries, different cloud fractions and different altitudes of the scattering cloud. In all cases a behavior similar to that shown in Figures 4 and 5 was found. In conclusion, the Lambertian cloud model with  $A_c = 0.8$  leads to small errors in total ozone of less than about 0.5%, as compared to a scattering cloud model.

### 3. OMI Cloud Algorithms Overview

[24] In section 2 we discussed the cloud model that is used in both OMI cloud algorithms. Here we present these

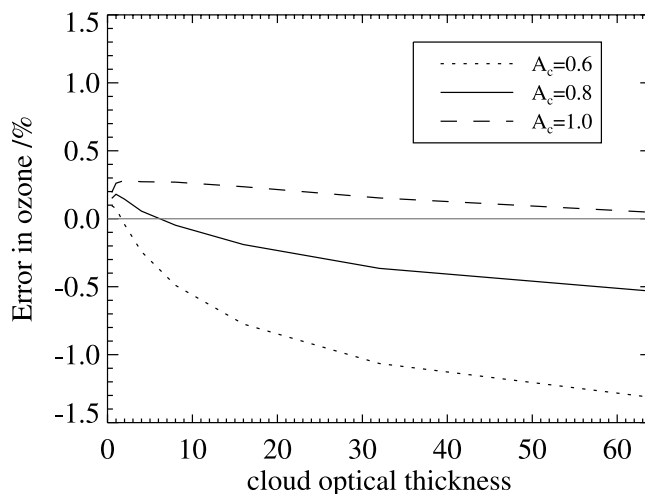


**Figure 5.** Error in the retrieved total ozone column (in %) due to the use of a Lambertian cloud model instead of a scattering cloud, as a function of cloud optical thickness, for the same cloudy scene and three Lambertian cloud retrieval models as used in Figure 4. The  $O_2-O_2$  cloud algorithm is used for the cloud pressure retrieval. The assumed ozone profile is a midlatitude summer profile with a total ozone column of 335 DU; 7.6% of the ozone column is located below 8 km, so 3.8% of ozone is below the cloud having  $c = 0.5$ .

algorithms in more detail, and end with a description of some differences between the two algorithms.

### 3.1. O<sub>2</sub>–O<sub>2</sub> Cloud Algorithm

[25] The OMI O<sub>2</sub>–O<sub>2</sub> algorithm uses the strongest oxygen absorption feature within the OMI wavelength range, which is the collision induced absorption (O<sub>2</sub>–O<sub>2</sub>) band at 477 nm. Since oxygen is well mixed, the detected amount of oxygen is a measure for the pressure of the reflecting boundary (surface or cloud). A Differential Optical Absorption Spectroscopy (DOAS) [Platt, 1994] fit on the OMI reflectance spectrum between 460 and 490 nm is used to determine the slant column amount of O<sub>2</sub>–O<sub>2</sub> and the continuum reflectance. Both quantities, combined with the viewing and solar geometry and surface conditions, are used to find the effective cloud fraction and cloud pressure with the aid of a lookup table. The lookup table was produced with the multiple scattering model DAK [de Haan et al., 1987; Stammes, 2001] including polarization, using a Lambertian surface as the cloud model. The surface albedo in the retrieval is taken from the GOME albedo database [Koelemeijer et al., 2003], in combination with the TOMS albedo database [Herman and Celarier, 1997]. Details of the OMI O<sub>2</sub>–O<sub>2</sub> cloud retrieval algorithm are given by Sneep et al. [2008] and Acarreta et al. [2004]. The O<sub>2</sub>–O<sub>2</sub> algorithm has been tested on GOME data [Acarreta et al., 2004].

[26] Simulations of the O<sub>2</sub>–O<sub>2</sub> retrieval method for a wide range of Mie scattering clouds, and for representative OMI viewing and solar geometries, have shown that the retrieved pressure of the cloud is about the midlevel of the cloud [Sneep et al., 2008; Acarreta and de Haan, 2002], even for optically thick clouds. This is important to realize when comparing with other cloud remote sensing methods.

### 3.2. Rotational Raman Scattering Cloud Algorithm

[27] The OMI RRS cloud algorithm uses inelastic Rotational Raman scattering (RRS) by N<sub>2</sub> and O<sub>2</sub> air molecules, which causes a wavelength-dependent redistribution of energy, also referred to as filling-in of spectral features (solar Fraunhofer lines or atmospheric absorption lines) in reflected light from the Earth [e.g., Joiner and Bhartia, 1995; Joiner et al., 1995]. Rotational Raman scattering is a small fraction (about 4%) of Rayleigh scattering, and is therefore strongest in the ultraviolet. The amount of filling-in is related to the number of Rayleigh scatterings encountered, which is a measure of the amount of air (or pressure) of the scene. Accurate models for RRS filling-in have been developed and compared well with observations from TOMS, SBUV, GOME, and ground-based measurements [Vasilkov et al., 2008]. The RRS cloud products are generated assuming a fixed surface albedo of 0.15; this was chosen to be consistent with the OMI total ozone retrieval based on the Total Ozone Mapping Spectrometer (TOMS) version 8 algorithm. The RRS algorithm has been applied to GOME and OMI [Joiner et al., 2004; Vasilkov et al., 2004; Joiner and Vassilkov, 2006]. The current OMI RRS algorithm uses a spectral fitting method for Raman filling-in in the range 345–354 nm [Vasilkov et al., 2008].

[28] Radiative transfer simulations of the RRS process by means of the LIDORT-RRS model [Spurr et al., 2007] and retrieval for Henyey-Greenstein scattering clouds by Vasilkov

et al. [2008] show that the retrieved cloud pressure is not the top of the cloud but a level inside the cloud for optically thick clouds. For a two-layer cloud system the retrieved pressure lies generally between the two cloud layers. However, under some conditions, the retrieved cloud pressure could be greater than that of the lower cloud due to enhanced scattering between the cloud decks. Significant errors may occur in retrieved cloud top pressure for thin clouds, especially those at high altitudes. The size and sign of the error vary with the viewing geometry but most importantly with the solar zenith angle [Vasilkov et al., 2008].

### 3.3. Algorithm Differences

[29] The physical principle of the OMI cloud algorithms is a photon path length determination using a spectral feature of a well-mixed atmospheric species, namely, oxygen, and nitrogen. However, the physical process of O<sub>2</sub>–O<sub>2</sub> and RRS cloud retrieval is different: one is based on absorption, while the other is based on scattering. The O<sub>2</sub>–O<sub>2</sub> absorption method includes all photon paths through the atmosphere, including the path of the direct solar beam to the surface and reflected back to the satellite. The RRS scattering method includes all atmospheric Rayleigh scattering paths but does not include the path of the direct solar beam to the surface (ground or cloud particle) and back to the satellite. Thus, the two methods will have a different impact of surface reflection on cloud pressure. This also means that the algorithms will behave differently when surfaces are non-Lambertian. For example, in the case of Sun glint on the ocean surface the RRS algorithm will be biased to low pressures, while the O<sub>2</sub>–O<sub>2</sub> algorithm will be biased to high pressures.

[30] The OMCLDRR algorithm uses the fixed cloud albedo of 0.8 only when the effective cloud fraction is less than 1. For very bright clouds, when the effective cloud fraction would exceed 1, the effective cloud fraction is set to 1 and the cloud albedo is increased to match the TOA reflectance. In these cases the OMCLDO2 algorithm keeps the cloud albedo at 0.8, but increases the effective cloud fraction to values above 1 to match the TOA reflectance. Both approaches can be used in the cloud correction of trace gas retrievals, because the cloud reflectance weight  $w$ , given by equation (7), is the product of effective cloud fraction and cloud albedo; this product is the same in both approaches.

[31] The OMCLDRR algorithm does not attempt a cloud pressure retrieval when the effective cloud fraction falls below 0.05. Instead, for diagnostic purposes, the effective scene pressure is given; this is the pressure of a bright Lambertian cloud completely filling the pixel which explains the observed RRS filling-in.

## 4. Comparison of O<sub>2</sub>–O<sub>2</sub> and RRS Effective Cloud Fractions

### 4.1. Data Selection

[32] In order to compare the two OMI cloud products for a large data set to get statistically meaningful results, we chose 1 d of global data, 2 August 2006. One day is about 1.5 million OMI pixels (for solar zenith angles <88°). Since we directly compare the L2 products from the same OMI

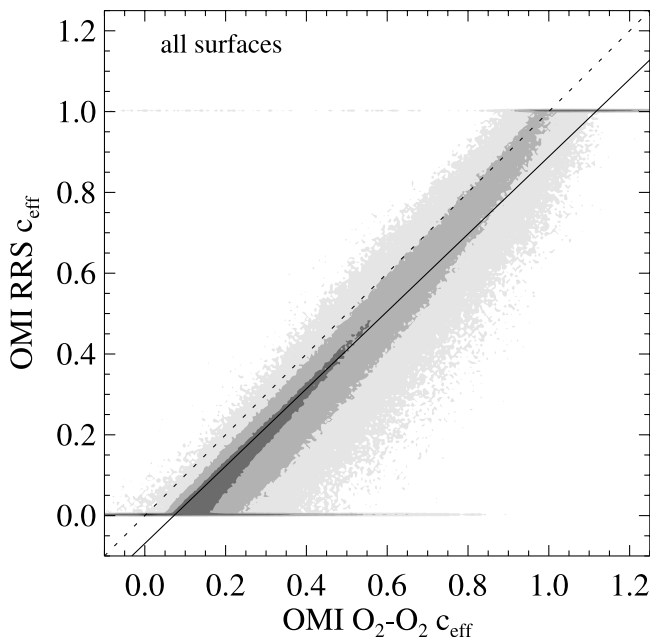


**Figure 6.** Correlation of the OMI  $O_2-O_2$  absorption and OMI rotational Raman scattering (RRS) effective cloud fractions for the global data of 2 August 2006. Please note that the RRS effective cloud fraction is clipped between 0 and 1. All surface types are included, except snow/ice. The solid line gives the straight-line fit to the data points. The correlation coefficient is  $r = 0.959$  with  $\sigma = 0.082$ . The grey scale indicates the density of data points in a logarithmic sense. The dotted line gives the 1:1 relation between both data sets.

pixels, we have no collocation problems. There is only a small coalignment difference, because the OMCLDRR and OMCLDO2 algorithms use fitting windows from two different detectors, namely, UV2 and VIS, respectively. These detectors have an alignment difference of 0.6 km at nadir, increasing toward the edges of the swath. Typically, the alignment difference is about 1 km, which is a few percent of the pixel size. This will give a small contribution to the scatter in the comparison.

[33] Here we use the  $O_2-O_2$  cloud product (OMCLDO2) version 1.0.1.1 and the RRS cloud product (OMCLDRR) version 1.2.0. From the cloud product OMCLDRR, the “Cloud Fraction for  $O_3$ ” value is used, because there the cloud albedo has been set to 0.8. The “Cloud Fraction” product in OMCLDRR uses a cloud albedo of 0.4 that produces a cloud fraction that is closer to the MODIS geometrical cloud fraction, but produces a deviating cloud pressure [Vasilkov *et al.*, 2008].

[34] The cloud data were filtered to exclude pixels over snow or ice covered surfaces. For those scenes it is known that the contrast between cloud cover and the surface is too low to properly distinguish clouds from the background, leading to an incorrect effective cloud fraction. The snow/ice flag is known to occasionally miss some snow/ice-covered pixels. This will give a small contribution to the scatter in the comparison. The total number of pixels used in the comparison was about 750,000.

## 4.2. Results

[35] The statistics of the comparison and of the individual  $O_2-O_2$  and RRS products have been produced with the CAMA software [Sneep, 2006]. The correlation between the two effective cloud fractions from the same pixels is shown in Figure 6.

[36] Although the correlation is very high (0.959), we notice a shift to the right, i.e., larger values for the effective cloud fraction from  $O_2-O_2$  than from RRS. There are two possible reasons: (1) the spectral dependence of  $c_{\text{eff}}$  as discussed in section 2.2, which can explain a shift of about 0.04 at most; and (2) the different surface albedo assumptions of the two products. The  $O_2-O_2$  algorithm uses the GOME/TOMS albedo database, whereas the RRS algorithm uses a constant surface albedo of 0.15 to be consistent with the OMI TOMS v8 algorithm. Because this albedo value is higher in general than the actual albedo of the surface in the UV (which is typically 0.05–0.10), it produces effective cloud fractions that are too low, especially for low scene reflectances.

[37] The global distribution functions of the two effective cloud fractions from OMI are shown in Figure 7. The  $O_2-O_2$  effective cloud fraction can lie between  $-0.2$  and  $1.5$ , whereas the RRS effective cloud fraction is clipped between 0 and 1. Many scenes with little or no clouds which would have a negative effective cloud fraction in the RRS algorithm, have a zero cloud fraction due to clipping; this occurs for 39% of all RRS cloud data points. To avoid the effect of the peaks at 0 and 1 on the comparison of the distributions, Figure 7 shows only the RRS pixels with  $0 < c_{\text{eff}} < 1$ . Here the RRS distribution function is scaled to the  $O_2-O_2$  distribution function for reason of comparison. We see reasonable agreement between the distributions but observe a shift toward lower cloud fractions in the RRS distribution, as may be caused by a too high surface albedo. Figure 8 shows the

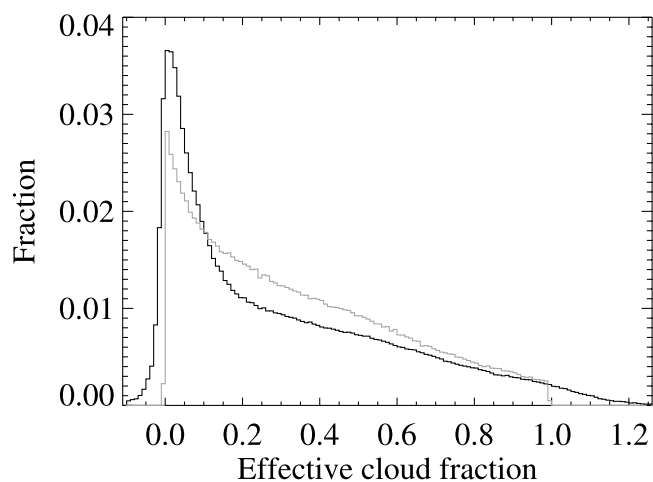


**Figure 7.** Distribution functions of the OMI  $O_2-O_2$  (black curve) and RRS (grey curve) effective cloud fractions for the same day of global data as shown in Figure 6. Since the RRS effective cloud fraction is clipped between 0 and 1, the resulting peaks at  $c_{\text{eff}} = 0$  and  $c_{\text{eff}} = 1$  have been omitted, and the RRS distribution has been scaled to the  $O_2-O_2$  distribution for reason of comparison.

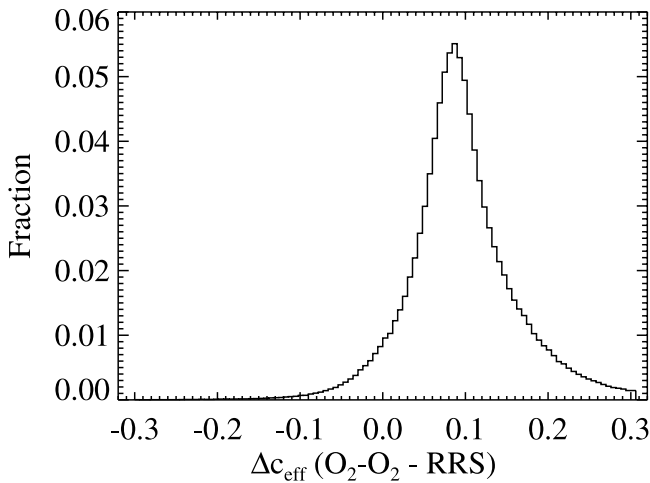


**Figure 8.** Distribution of the pixel-to-pixel differences between the  $O_2-O_2$  and RRS effective cloud fractions. The mean difference in effective cloud fraction between  $O_2-O_2$  and RRS, excluding the clipped pixels, is 0.104 and the standard deviation is 0.077.

distribution of the pixel-to-pixel differences in  $c_{\text{eff}}$  between  $O_2-O_2$  and RRS. The average difference is 0.104 (0.097 for land and 0.106 for ocean), excluding the clipped RRS data points.

[38] The global mean effective cloud fraction is 0.305 from  $O_2-O_2$ , and 0.223 from RRS. This is a difference of 0.082, which is somewhat lower than the above pixel-by-pixel comparison result of 0.104 due to contribution of the RRS points having  $c_{\text{eff}} = 0$ . The standard deviation in the mean effective cloud fraction is 0.295 for  $O_2-O_2$  and 0.283 for RRS. The global mean effective cloud fraction from SCIAMACHY (FRESCO algorithm) is 0.31, for monthly

averaged data for August 2004 and 2005, so very similar to the OMI  $O_2-O_2$  global mean effective cloud fraction; the small difference agrees with the expected spectral dependence of the  $c_{\text{eff}}$  (compare section 2.2). The good agreement is not surprising, because of the large amount of pixels used and the statistically robust radiometric properties of clouds if globally averaged.

[39] The effective cloud fraction comparisons between  $O_2-O_2$  and RRS for global data and for land and ocean separately are summarized in Table 1.

## 5. Comparison of OMCLDO2 and MODIS Cloud Fractions

[40] As a validation of OMI, we performed a global comparison of the OMI  $O_2-O_2$  effective cloud fraction with cloud products from the moderate resolution imaging spectrometer (MODIS) on EOS-Aqua. Both Aura, the platform hosting OMI, and Aqua are part of the “A” train, a series of satellites flying in formation, and crossing the equator in the early afternoon. Because of the formation flying, OMI and MODIS cover almost the same ground track within about 15 min, with comparable swath widths (2330 km for MODIS, 2600 km for OMI).

[41] MODIS is a 36-channel imaging spectrometer [King *et al.*, 1992; Platnick *et al.*, 2003], producing a wide range of products, of which the cloud mask and the cloud optical thickness are used here. MODIS is an obvious choice for comparison with the OMI cloud products given its capability for cloud detection and high spatial resolution ( $1 \times 1 \text{ km}^2$ ).

### 5.1. Mapping MODIS Measurements Onto the OMI Measurement Grid

[42] OMI and MODIS have different grids for the level 2 (orbit) data. Although it is tempting to compare the regridded level 3 products of OMI and MODIS on a regular latitude and longitude grid, there is a severe disadvantage to

**Table 1.** Summary of OMI Cloud Validation Results for Effective Cloud Fraction  $c_{\text{eff}}$  and Cloud Pressure  $p_c$  as Presented in This Special Section<sup>a</sup>

Quantity	Product	Comparison	Area	Period	Data Range	$r$	$\Delta$	$\sigma$	Notes <sup>b</sup>
$c_{\text{eff}}$	$O_2-O_2$	RRS	global	day	all; not clipped	0.959	0.082	0.084	a
$c_{\text{eff}}$	$O_2-O_2$	RRS	global	day	all; $0.0 < c_{\text{eff}} < 1.0$	0.952	0.104	0.077	a
$c_{\text{eff}}$	$O_2-O_2$	RRS	global	day	land; $0.0 < c_{\text{eff}} < 1.0$	0.954	0.097	0.082	a
$c_{\text{eff}}$	$O_2-O_2$	RRS	global	day	ocean; $0.0 < c_{\text{eff}} < 1.0$	0.951	0.106	0.076	a
$c_{\text{eff}}$	$O_2-O_2$	MODIS	global	day	all; $c_{\text{eff}}^{\text{MODIS}} > 0.01$	0.915	0.008	0.12	a
$p_c$	$O_2-O_2$	RRS	global	month	all; $c_{\text{eff}} > 0.5$	0.92	44 hPa	65 hPa	b
$p_c$	$O_2-O_2$	RRS	global	month	land; $c_{\text{eff}} > 0.5$	0.89	46 hPa	66 hPa	b
$p_c$	$O_2-O_2$	RRS	global	month	ocean; $c_{\text{eff}} > 0.5$	0.92	45 hPa	66 hPa	b
$p_c$	$O_2-O_2$	PARASOL	global	month	all; $c_{\text{eff}} > 0.5$	0.93	45 hPa	74 hPa	b
$p_c$	$O_2-O_2$	PARASOL	global	month	land; $c_{\text{eff}} > 0.5$	0.91	30 hPa	73 hPa	b
$p_c$	$O_2-O_2$	PARASOL	global	month	ocean; $c_{\text{eff}} > 0.5$	0.93	47 hPa	75 hPa	b
$p_c$	RRS	PARASOL	global	month	all; $c_{\text{eff}} > 0.5$	0.88	2 hPa	93 hPa	b
$p_c$	RRS	PARASOL	global	month	land; $c_{\text{eff}} > 0.5$	0.84	-17 hPa	92 hPa	b
$p_c$	RRS	PARASOL	global	month	ocean; $c_{\text{eff}} > 0.5$	0.89	2 hPa	95 hPa	b
$p_c$	$O_2-O_2$	CloudSat	regional	<day	$c_{\text{eff}} > 0.2$	N/A	cloud middle	N/A	b
$p_c$	RRS	CloudSat	regional	<day	$c_{\text{eff}} > 0.2$	N/A	cloud middle	N/A	b, c
$p_c$	$O_2-O_2$	MODIS	regional	<day	$c_{\text{eff}} > 0.2$	N/A	100–500 hPa	N/A	b
$p_c$	RRS	MODIS	regional	<day	$c_{\text{eff}} > 0.2$	N/A	100–500 hPa	N/A	b, c

<sup>a</sup>The OMI  $O_2-O_2$  cloud product (OMCLDO2) is indicated by  $O_2-O_2$  and the OMI Raman cloud product (OMCLDRR) is indicated by RRS. The used RRS cloud parameters are CloudFractionfor $O_3$  and CloudPressurefor $O_3$ ;  $r$  is the correlation coefficient,  $\Delta$  is the mean difference (column 2 minus column 3), and  $\sigma$  is the standard deviation of  $\Delta$ . Snow and ice scenes were excluded. N/A means not available.

<sup>b</sup>Sources are a, this paper; b, Sneep *et al.* [2008]; and c, Vasilkov *et al.* [2008].

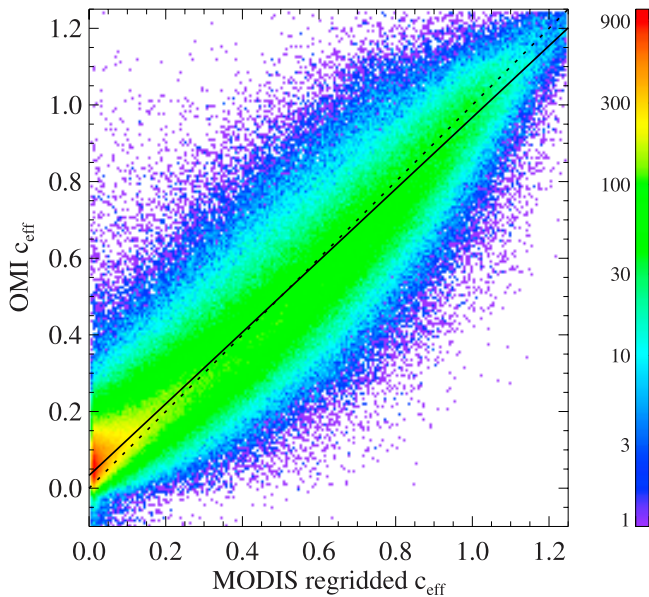


**Figure 9.** Correlation between the OMI O<sub>2</sub>–O<sub>2</sub> effective cloud fraction and the calculated MODIS effective cloud fraction, based on the MODIS cloud optical thickness, regridded to the OMI grid. This analysis contains the global data of 2 August 2006. The color scale indicates the density of measurements at each coordinate in the plot. The solid line is the regression line, showing an offset of 0.034 between the data sets, at a slope of 0.934. The correlation coefficient, excluding data points with an effective cloud fraction smaller than 0.01 in the MODIS data, is 0.915. The dotted line gives the 1:1 relation between both data sets.

such an approach: the time difference between OMI and MODIS is not used at all, which can result in comparing measurements that are several hours apart, rather than the 15 min between the overpasses. This may cause large deviations, especially for clouds. In our analysis we therefore mapped the MODIS level 2 data onto the OMI level 2 measurement grid and compared the level 2 data directly. Given the difference in pixel size ( $1 \times 1 \text{ km}^2$  for MODIS and  $13 \times 24 \text{ km}^2$  for OMI, both for nadir observations), the MODIS pixels are considered to match an OMI pixel if their centers fall within the OMI pixel. Because of the variation in the pixel size of both instruments as a function of the viewing direction, and the offset of the ground tracks, about 200 MODIS pixels match a single OMI pixel on the west side of the swath, while on the east side of the swath about 400 matching MODIS pixels are found.

## 5.2. Obtaining an Effective Cloud Fraction From MODIS Measurements

[43] The OMI effective cloud fraction  $c_{\text{eff}}$  is not a geometrical cloud fraction as retrieved by MODIS, but it is a combination of geometric cloud fraction, cloud reflectance, and clear sky reflectance (see equation (6)). As such there is no direct method to compare the OMI  $c_{\text{eff}}$  with an existing MODIS product. We therefore converted the MODIS level 2 cloud optical thickness, which is given at 650 nm [King *et al.*, 1998], into a cloud reflectance, and

computed the effective cloud fraction from the cloud reflectance and geometric cloud fraction in an approximate way. In the MODIS cloud optical thickness product, the geometric cloud fraction is implicitly included, and takes values of either 1 (if there is a cloud) or 0 (if no clouds are detected). A lookup table of the cloud reflectance as a function of the MODIS cloud optical thickness was created using the DAK model. Since we had no information on the MODIS clear sky reflectance, we used an approximation of equation (6) by neglecting the clear sky reflectance and the atmospheric and surface contributions to the cloud reflectance. For the lookup table an isolated scattering cloud layer, consisting of Mie scattering particles at 470 nm, using the C1 cloud droplet size distribution [Deirmendjian, 1969] with effective radius of  $6 \mu\text{m}$ , was assumed. The calculated cloud reflectances were averaged over the OMI pixel and divided by 0.8, which is the albedo of our Lambertian cloud model, to obtain the calculated MODIS effective cloud fraction for the OMI pixel:

$$c_{\text{eff}}^{\text{MODIS},j} = \frac{1}{N_{\text{match}}^j} \sum_i^{N_{\text{match}}^j} \frac{R_c(\tau_c^{\text{(MODIS)},i})}{0.8} \quad (8)$$

with  $j$  an index for the OMI pixel,  $N_{\text{match}}^j$  the number of matching MODIS pixels, and  $c_{\text{eff}}^{\text{MODIS},j}$  the MODIS effective cloud fraction on the OMI grid. Here  $R_c$  indicates that only the cloud reflectance itself is considered, without atmospheric scattering and surface reflection.

[44] We computed the error due to the neglect of atmospheric scattering and surface reflection in equation (8) as compared to the definition of the effective cloud fraction in equation (6). For a surface albedo of 0.05, as used in Figure 3, the difference in  $c_{\text{eff}}$  at 470 nm between neglect and inclusion of atmospheric scattering and surface reflection is  $<0.025$  for  $\tau_c < 30$ .

## 5.3. Comparing the Effective Cloud Fractions of OMI and MODIS

[45] A little over a day of OMI and MODIS global measurements is used in this intercomparison, 16 orbits in total (OMI orbits 10889 through 10904). Over this period almost  $9 \times 10^5$  matching measurements were performed, which is 60% of the total number of OMI measurements during that period. The day used for this comparison is 2 August 2006.

[46] For the intercomparison, MODIS collection 005 data are used, processed with software version 5.11.0. The OMI data (level 1B to level 2) are processed with software version 1.0.1.1, while the level 1B data are produced by software version 0.9.15.2.

[47] For the chosen day the correlation between  $c_{\text{eff}}$  from OMI and from MODIS is shown in Figure 9. When excluding pixels with  $c_{\text{eff}}^{\text{MODIS}} < 0.01$ , we find a correlation coefficient between the two data sets of 0.92. When we include these pixels the correlation is even higher, but this is rather artificial, as this includes a large number of data points at  $c_{\text{eff}} = 0$  in both sets. The drawn line in Figure 9 is a straight line fit to the measurements, assuming a constant error of  $1\sigma = 0.08$  on both sets, and using a fitting technique which includes errors on both the OMI and MODIS measurements in the analysis [Press *et al.*, 1992, section 15.3].

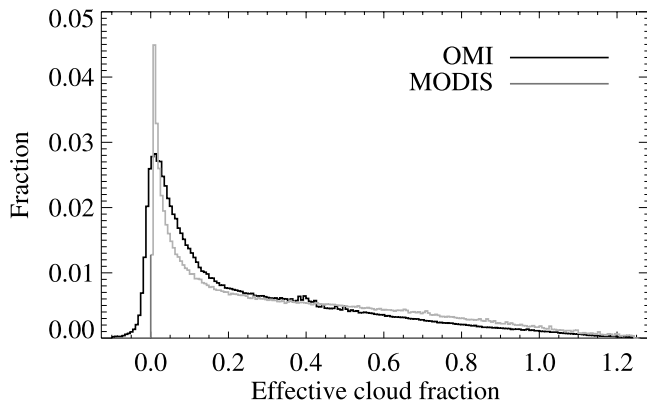


**Figure 10.** Distribution functions of the effective cloud fraction from OMI  $O_2-O_2$  (black curve) and MODIS (grey curve), for the same data as shown in Figure 9.

With this technique we find an offset of 0.03 between the data sets, at a slope of 0.93. The relation between the OMI and MODIS effective cloud fractions is not completely linear, as can be seen in Figure 9. For small cloud fractions the surface albedo plays a role, and this seems to yield slightly higher effective cloud fractions for OMI compared to MODIS. The distribution of effective cloud fractions of both instruments is shown in Figure 10. The occurrence of slightly negative effective cloud fractions in OMI (in about 7% of all cases) is due to the fact that the surface albedo database used in the retrieval has a much coarser resolution ( $1^\circ \times 1^\circ$ ) than the observations. The occurrence of effective cloud fractions larger than 1 is due to the fact that cloud reflectances may be larger than 0.8. The distribution of the pixel-to-pixel differences in  $c_{\text{eff}}$ , again without  $c_{\text{eff}}^{\text{MODIS}} < 0.01$ , is shown in Figure 11. The  $1\sigma$  width of the distribution of differences is 0.12, and the average difference is 0.008. The cloud model that has been used to convert MODIS cloud optical thickness values into cloud reflectance values is probably not correct for all clouds, and may explain the standard deviation of 0.12.

[48] The distribution of effective cloud fractions from OMI and MODIS hardly changed when we used 7 orbits instead of 14 orbits. Therefore, the distributions shown above have converged for the 14 orbits (full day of data) that we have used.

[49] The previous comparisons were performed without pixels that have a NISE indicated snow or ice cover larger than 5% [Nolin *et al.*, 2005]. When the comparison focusses on scenes classified with snow or ice on the surface, we find some rather different results. The correlation between the OMI and MODIS  $c_{\text{eff}}$  drops to 0.39, while the  $1\sigma$  spread of the distribution of differences becomes much wider, namely, 0.28. This is caused by the lack of contrast between snow/ice surface and clouds, making it impossible to determine accurate cloud fractions from OMI measurements.

## 6. Discussion and Conclusions

[50] The simplified Lambertian cloud model, often used for cloud correction of trace gas retrievals from OMI and other UV-visible satellite spectrometers like GOME,

SCIAMACHY and GOME-2, has been motivated. The rationale of the assumed cloud albedo of 0.8 is to reproduce both the reflection and transmission properties of a cloudy pixel. The Lambertian cloud model has two free parameters: effective cloud fraction and cloud pressure. The effective cloud fraction is a radiometric cloud fraction, mainly depending on geometric cloud fraction and cloud optical thickness but also on the clear sky reflectance. Owing to this latter dependence we find a slight spectral dependence of the effective cloud fraction. Therefore, the effective cloud fraction for trace gas correction should be used from a nearby spectral window. Because of multiple scattering, the cloud pressure of the Lambertian cloud model is a level inside the cloud. For cloud correction of total ozone, we find that the Lambertian cloud model with albedo 0.8 gives errors of less than about 0.5% as compared to a scattering cloud model.

[51] We intercompared the effective cloud fractions from the  $O_2-O_2$  and RRS products globally, and found a high correlation (95%), but an offset of about 0.1. This can most likely be explained by the combination of spectral dependence of the effective cloud fraction and the too high surface albedo used in the current RRS algorithm. Both OMI cloud algorithms will use updated surface albedo climatologies in subsequent versions, which is expected to bring  $O_2-O_2$  and RRS effective cloud fractions and cloud pressures into better agreement, especially for lower cloud fractions. Updated albedo climatologies should also be used in the trace gas retrieval algorithms in order to improve air mass factor calculations and to maintain consistency with cloud retrievals.

[52] We compared the  $O_2-O_2$  effective cloud fraction with MODIS data; thereto, a MODIS effective cloud fraction was calculated from the MODIS cloud optical thickness. The correlation between OMI  $O_2-O_2$  and MODIS effective cloud fractions was very good (92%), with a mean difference of about 0.01 and standard deviation of 0.12.

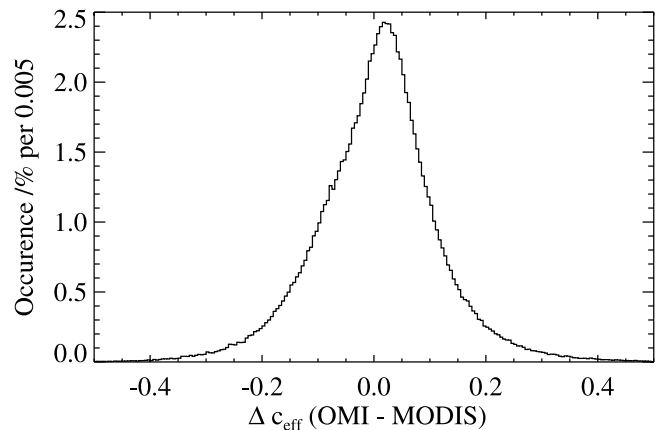


**Figure 11.** Distribution of the pixel-to-pixel differences between the  $O_2-O_2$  and MODIS effective cloud fractions. To calculate the difference in the effective cloud fraction,  $\Delta c_{\text{eff}}$ , between OMI and MODIS, cloud-free pixels and pixels with snow or ice were excluded. The mean difference is 0.008, and the standard deviation is 0.12.

[53] A summary of all the OMI cloud validation results presented in this special section, including cloud pressure, is given in Table 1. The cloud pressure comparison results between OMI  $O_2-O_2$ , OMI RRS and PARASOL/POLDER, and between OMI  $O_2-O_2$  and MODIS are mainly shown for effective cloud fractions larger than 0.5; this selects mostly cloudy pixels, since comparisons for pixels with broken clouds are more ambiguous. Table 1 shows that the average cloud pressure differences are small ( $-3$  to  $46$  hPa) for all methods which operate in the UV-visible and use a Lambertian cloud model, namely, OMI  $O_2-O_2$ , OMI RRS, and PARASOL/POLDER, which uses the  $O_2$  A band at  $760$  nm. The POLDER cloud pressure has been validated before with ground-based radar/lidar data [Vanbauce *et al.*, 1998, 2003], where it was found that the retrieved cloud pressure indicates the midlevel of the cloud. However, this was a limited set of data points, inherent when using ground-based observations during satellite overpass as validation technique. With the A-train collocations, especially with CloudSat, the statistics for cloud pressure validation has increased enormously. The comparison between OMI and MODIS cloud pressures [Sneep *et al.*, 2008; Vasilkov *et al.*, 2008] shows large differences, of the order of  $100-500$  hPa, with the OMI cloud pressures being higher. MODIS, operating in the thermal IR, yields the top of the cloud, whereas OMI detects a level inside the cloud, close to the middle. This is confirmed by the OMI-CloudSat comparisons presented by Sneep *et al.* [2008] and Vasilkov *et al.* [2008].

[54] These comparisons show that the retrieved OMI cloud pressure, either by  $O_2-O_2$  or RRS, is not the top of the cloud, but a level inside the cloud, typically near the middle. For ozone and other trace gas retrievals it is essential to use the right altitude of the cloud that is used in the cloud correction approach. In most cloud correction algorithms, the cloud is assumed to be an opaque Lambertian reflector. If the altitude of this cloud is too high, there is too much ghost column added to the measured column amount, leading to a too high total ozone or other trace gas column. This holds for retrieval algorithms which use ghost columns for the “unseen” trace gas column.

[55] One of the most important results of the OMI total ozone validation using two different total ozone algorithms, namely, TOMS and DOAS [Kroon *et al.*, 2008] is that the TOMS ozone column is on average too high over clouds. This can be explained by the fact that the TOMS version 8 algorithm uses a climatology of cloud pressure as measured by the thermal IR sensor (THIR) on board Nimbus 7. As was found from OMI cloud comparisons with MODIS IR data [Sneep *et al.*, 2008], OMI yields a lower cloud altitude (higher pressure) than MODIS. Apparently, the right altitude for ozone cloud correction is the middle of the cloud and not the top. This was corroborated by radiative transfer simulations of ozone retrieval in the case of scattering clouds presented in section 2.3.

[56] The error in TOMS version 8 total ozone by using climatological IR cloud heights instead of observed UV cloud heights was already noted by Vasilkov *et al.* [2004] and Joiner and Vassilkov [2006]. Previous analyses of effects of clouds on TOMS total ozone suggested that the Lambertian cloud model was the source of error [Liu *et al.*, 2004; Newchurch *et al.*, 2001].

[57] However, we propose that the use of the Lambertian cloud model in trace gas retrievals is able to produce accurate results if the Lambertian cloud is placed at around the optical midlevel of the physical cloud, i.e., the pressure level that is reported by the OMI cloud products. Only the consistent use of cloud model assumptions between cloud and trace gas retrievals assures optimal results that will contribute to the improvement of ozone and tropospheric air quality monitoring from satellite.

[58] **Acknowledgments.** OMI is a contribution of the Netherlands' Agency for Aerospace Programs (NIVR) in collaboration with the Finnish Meteorological Institute (FMI) to NASA's EOS-Aura satellite. The OMI science team is gratefully acknowledged for the satellite data used in this study. The work at KNMI has been partially funded by the Space Research Organisation of the Netherlands (SRON) under grants EO-067 and EO-072. Discussions with P. K. Bhartia, J. Joiner, and A. Vasilkov are gratefully acknowledged. We thank the anonymous reviewers for their constructive comments and suggestions.

## References

- Acarreta, J. R., and J. F. de Haan (2002), Cloud pressure algorithm based on  $O_2-O_2$  absorption, in *OMI Algorithm Theoretical Basis Document*, vol. III, *Clouds, Aerosols, and Surface UV Irradiance*, edited by P. Stammes, pp. 17–29, R. Neth. Meteorol. Inst., De Bilt.
- Acarreta, J. R., J. F. De Haan, and P. Stammes (2004), Cloud pressure retrieval using the  $O_2-O_2$  absorption band at  $477$  nm, *J. Geophys. Res.*, *109*, D05204, doi:10.1029/2003JD003915.
- Ahmad, Z., P. K. Bhartia, and N. Krotkov (2004), Spectral properties of backscattered UV radiation in cloudy atmospheres, *J. Geophys. Res.*, *109*, D01201, doi:10.1029/2003JD003395.
- Boersma, K. F., H. J. Eskes, and E. J. Brinksma (2004), Error analysis for tropospheric  $NO_2$  retrieval from space, *J. Geophys. Res.*, *109*, D04311, doi:10.1029/2003JD003962.
- Bovensmann, H., J. P. Burrows, M. Buchwitz, J. Frerick, S. Noël, V. V. Rozanov, K. V. Chance, and A. P. Goede (1999), SCIAMACHY: Mission objectives and measurement modes, *J. Atmos. Sci.*, *56*, 127–150, doi:10.1175/1520-0469(1999)056<0127:SMOAMM>2.0.CO;2.
- Burrows, J. P., et al. (1999), The Global Ozone Monitoring Experiment (GOME): Mission concept and first scientific results, *J. Atmos. Sci.*, *56*, 151–175, doi:10.1175/1520-0469(1999)056<0151:TGOMEG>2.0.CO;2.
- de Haan, J. F., P. B. Bosma, and J. W. Hovenier (1987), The adding method for multiple scattering calculations of polarized light, *Astron. Astrophys.*, *183*, 371–393.
- Deirmendjian, D. (1969), *Electromagnetic Scattering on Spherical Polydispersions*, Elsevier, New York.
- Herman, J. R., and E. A. Celarier (1997), Earth surface reflectivity climatology at  $340-380$  nm from TOMS data, *J. Geophys. Res.*, *102*(D23), 28,003–28,012, doi:10.1029/97JD02074.
- Joiner, J., and P. K. Bhartia (1995), The determination of cloud pressures from rotational Raman scattering in satellite backscatter ultraviolet measurements, *J. Geophys. Res.*, *100*(D11), 23,019–23,026.
- Joiner, J., and A. P. Vassilkov (2006), First results from the OMI rotational Raman scattering cloud pressure algorithm, *IEEE Trans. Geosci. Remote Sens.*, *44*(5), 1272–1282, doi:10.1109/TGRS.2005.861385.
- Joiner, J., P. K. Bhartia, R. P. Cebula, E. Hilsenrath, R. D. McPeters, and H. Park (1995), Rotational-Raman scattering (Ring effect) in satellite backscatter ultraviolet measurements, *Appl. Opt.*, *34*(21), 4513.
- Joiner, J., A. P. Vasilkov, D. E. Flittner, J. F. Gleason, and P. K. Bhartia (2004), Retrieval of cloud pressure and oceanic chlorophyll content using Raman scattering in GOME ultraviolet spectra, *J. Geophys. Res.*, *109*, D01109, doi:10.1029/2003JD003698.
- Joiner, J., A. Vasilkov, K. Yang, and P. K. Bhartia (2006), Observations over hurricanes from the Ozone Monitoring Instrument, *Geophys. Res. Lett.*, *33*, L06807, doi:10.1029/2005GL025592.
- King, M. D., Y. J. Kaufman, W. P. Menzel, and D. Tanré (1992), Remote sensing of cloud, aerosol, and water vapor properties from the Moderate Resolution Imaging Spectrometer (MODIS), *IEEE Trans. Geosci. Remote Sens.*, *30*(1), 1–27.
- King, M. D., S.-C. Tsay, S. E. Platnick, M. Wang, and K.-N. Liou (1998), Cloud retrieval algorithms for MODIS: Optical thickness, effective particle radius, and thermodynamic phase, *Tech. Rep. ATBD-MOD-05*, NASA, Washington, D. C.

- Koelemeijer, R. B. A., and P. Stammes (1999), Effects of clouds on ozone column retrieval from GOME UV measurements, *J. Geophys. Res.*, *104*(D7), 8281–8294, doi:10.1029/1999JD900012.
- Koelemeijer, R. B. A., P. Stammes, J. W. Hovenier, and J. F. de Haan (2001), A fast method for retrieval of cloud parameters using oxygen A-band measurements from GOME, *J. Geophys. Res.*, *106*(D04), 3475–3490, doi:10.1029/2000JD900657.
- Koelemeijer, R. B. A., J. F. de Haan, and P. Stammes (2003), A database of spectral surface reflectivity in the range 335–772 nm derived from 5.5 years of GOME observations, *J. Geophys. Res.*, *108*(D2), 4070, doi:10.1029/2002JD002429.
- Kokhanovsky, A. A., B. Mayer, V. V. Rozanov, K. Wapler, L. N. Lamsal, M. Weber, J. P. Burrows, and U. Schumann (2007), Satellite ozone retrieval under broken cloud conditions: An error analysis based on Monte Carlo simulations, *IEEE Trans. Geosci. Remote Sens.*, *45*, 187–194, doi:10.1109/TGRS.2006.886188.
- Krijger, J., M. van Weele, I. Aben, and R. Frey (2007), Technical note: The effect of sensor resolution on the number of cloudfree observations from space, *Atmos. Chem. Phys.*, *7*, 2881–2891.
- Kroon, M., J. P. Veefkind, M. Sneep, R. D. McPeters, P. K. Bhartia, and P. Levelt (2008), Comparing OMI-TOMS and OMI-DOAS total ozone column data, *J. Geophys. Res.*, doi:10.1029/2007JD008798, in press.
- Levelt, P. F., E. Hilsenrath, G. W. Leppelmeier, G. H. J. van den Oord, P. K. Bhartia, J. Tamminen, J. F. de Haan, and J. P. Veefkind (2006a), Science objectives of the Ozone Monitoring Instrument, *IEEE Trans. Geosci. Remote Sens.*, *44*(5), 1199–1208, doi:10.1109/TGRS.2006.872336.
- Levelt, P. F., G. H. J. van den Oord, M. R. Dobber, A. Malkki, H. Visser, J. de Vries, P. Stammes, J. Lundell, and H. Saari (2006b), The Ozone Monitoring Instrument, *IEEE Trans. Geosci. Remote Sens.*, *44*(5), 1093–1101, doi:10.1109/TGRS.2006.872333.
- Liu, X., M. J. Newchurch, R. Loughman, and P. K. Bhartia (2004), Errors resulting from assuming opaque lambertian clouds in TOMS ozone retrieval, *J. Quant. Spectrosc. Radiat. Transfer*, *85*, 337–365, doi:10.1016/S0022-4073(03)00231-0.
- McPeters, R., et al. (1996), Nimbus-7 Total Ozone Mapping spectrometer (TOMS) data products user's guide, *NASA Ref. Publ.*, 1384.
- Newchurch, M. J., X. Liu, J. H. Kim, and P. K. Bhartia (2001), On the accuracy of Total Ozone Mapping Spectrometer retrievals over tropical cloudy regions, *J. Geophys. Res.*, *106*, 32,315–32,326.
- Nolin, A., R. Armstrong, and J. Maslanik (2005), Near real-time SSM/I EASE-grid daily global ice concentration and snow extent, digital media, updated daily, Natl. Snow and Ice Data Cent., Boulder, Colo.
- Palmer, P. I., et al. (2001), Air mass factor formulation for spectroscopic measurements from satellites: Application to formaldehyde retrievals from the Global Ozone Monitoring Experiment, *J. Geophys. Res.*, *106*, 14,539–14,550.
- Platnick, S., M. King, S. Ackerman, W. Menzel, B. Baum, J. Riedi, and R. Frey (2003), The MODIS cloud products: Algorithms and examples from Terra, *IEEE Trans. Geosci. Remote Sens.*, *41*(2), 459–473, doi:10.1109/TGRS.2002.808301.
- Platt, U. (1994), Differential optical absorption spectroscopy (DOAS), in *Air Monitoring by Spectroscopic Techniques*, *Chem. Anal. Ser.*, vol. 127, edited by M. W. Sigrist, pp. 27–84, John Wiley, New York.
- Press, W. H., S. A. Teukolsky, W. T. Vetterling, and B. P. Flannery (1992), *Numerical Recipes in FORTRAN 77: The Art of Scientific Computing*, 2nd ed., Cambridge Univ. Press, New York.
- Sneep, M. (2006), Documentation for the 'CAMA' verification and validation toolkit, *OMI Doc. MA-OMIE-KNMI-832*, R. Neth. Meteorol. Inst., De Bilt, Netherlands.
- Sneep, M., J. F. De Haan, P. Stammes, P. Wang, C. Vanbauce, J. Joiner, A. Vasilkov, and P. Levelt (2008), Three-way comparison between OMI and PARASOL cloud pressure products, *J. Geophys. Res.*, *113*, D15S23, doi:10.1029/2007JD008694.
- Spurr, R., J. de Haan, R. van Oss, and A. Vasilkov (2007), Discrete ordinate radiative transfer in a stratified medium with first order rotational Raman scattering, *J. Quant. Spectrosc. Radiat. Transfer*, *109*, 404–425, doi:10.1016/j.jqsrt.2007.08.011.
- Stammes, P. (2001), Spectral radiance modeling in the UV-visible range, in *IRS2000: Current Problems in Atmospheric Radiation*, edited by W. L. Smith and Y. M. Timofeyev, pp. 385–388, A. Deepak, Hampton, Va.
- Vanbauce, C., J. Buriez, F. Parol, B. Bonnel, G. Sèze, and P. Couvert (1998), Apparent pressure derived from ADEOS-POLDER observations in the oxygen A-band over ocean, *Geophys. Res. Lett.*, *25*(16), 3159–3162.
- Vanbauce, C., B. Cadet, and R. T. Marchand (2003), Comparison of POLDER apparent and corrected oxygen pressure to ARM/MMCR cloud boundary pressures, *Geophys. Res. Lett.*, *30*(5), 1212, doi:10.1029/2002GL016449.
- van de Hulst, H. C. (1980), *Multiple Light Scattering. Tables, Formulas, and Applications*, vols. 1 and 2, Academic, New York.
- Van Roozendaal, M., et al. (2006), Ten years of GOME/ERS-2 total ozone data-The new GOME data processor (GDP) version 4: 1. Algorithm description, *J. Geophys. Res.*, *111*, D14311, doi:10.1029/2005JD006375.
- Vasilkov, A. P., J. Joiner, K. Yang, and P. K. Bhartia (2004), Improving total column ozone retrievals by using cloud pressures derived from Raman scattering in the UV, *Geophys. Res. Lett.*, *31*, L20109, doi:10.1029/2004GL020603.
- Vasilkov, A., J. Joiner, R. J. D. Spurr, P. K. Bhartia, P. Levelt, and G. Stephens (2008), Evaluation of the OMI cloud pressures derived from rotational Raman scattering by comparisons with other satellite data and radiative transfer simulations, *J. Geophys. Res.*, *113*, D15S19, doi:10.1029/2007JD008689.
- Veefkind, J. P., J. F. de Haan, E. J. Brinksma, M. Kroon, and P. F. Levelt (2006), Total ozone from the Ozone Monitoring Instrument (OMI) using the DOAS technique, *IEEE Trans. Geosci. Remote Sens.*, *44*(5), 1239–1244, doi:10.1109/TGRS.2006.871204.
- Wang, P., P. Stammes, and K. F. Boersma (2006), Impact of the effective cloud fraction assumption on tropospheric NO<sub>2</sub> retrievals, in *Proceedings of the First Conference on Atmospheric Science, Eur. Space Agency Spec. Publ.*, ESA SP-628, Abstract p4\_38.

J. F. de Haan, P. F. Levelt, M. Sneep, P. Stammes, J. P. Veefkind, and P. Wang, Climate Research and Seismology Department, Royal Netherlands Meteorological Institute, P.O. Box 201, NL-3730 AE De Bilt, Netherlands. (stammes@knmi.nl)